Electronic Supplementary Material (ESI) for Physical Chemistry Chemical Physics.

Supporting Information

for

Quantitative description of ^{1}H SQ and DQ coherences for the hydroxyl disorder within hydrous ringwoodite

Helen Grüninger,[a] Adrian Schmutzler,[a] Renée Siegel,[a] Katherine Armstrong,[b] Daniel J. Frost[b] and Jürgen Senker*[a]

[a] Anorganische Chemie III, University of Bayreuth, Universitätsstr. 30, 95447 Bayreuth, Germany.

[b] Bayerisches Geo-Institut, University of Bayreuth, Universitätsstr. 30, 95447 Bayreuth, Germany.

*juergen.senker@uni-bayreuth.de

Contents

1. Influence of the CSA on experimental spectra and simulations

The occurrence of spinning sidebands as shown in Fig. S1 indicate a significant contribution of the chemical shift anisotropy. We observe a slightly poorer resolution in the spinning sidebands, which is a common phenomenon for MAS NMR spectroscopy. In our case a likely explanation is a higher spin correlation in some defect types, as previously described by Schnell and Spiess[1] and Zorin *et al.*[2].

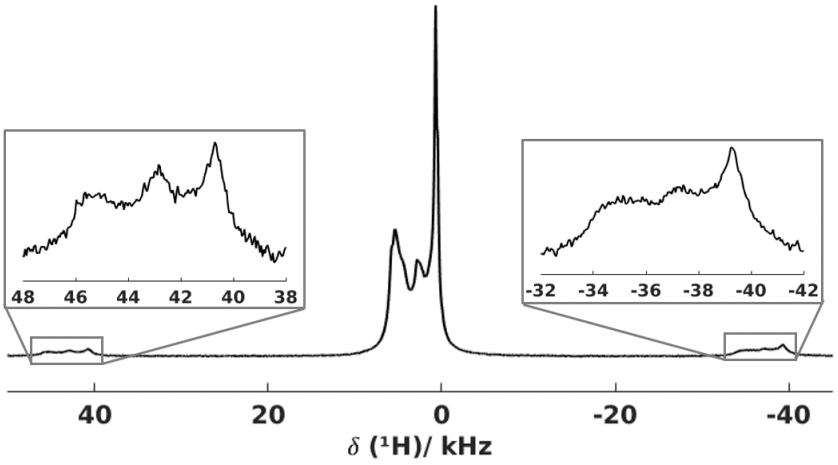

Fig. S1: ^{1}H MAS spin-echo of hydrous ringwoodite with two visible spinning sidebands ($\nu_{rot.}$ 40 kHz) highlighted as insets. The presence of two spinning sidebands with comparable lineshapes indicates a CSA of significant strength for all defect types and emphasizes the necessity to consider the CSA interaction in the simulations of experimental observables.

Two different two-spin systems of an isolated Mg vacancy (V_{Mg}''+ 2H**) with varying strength of the CSA were used (Table S1) to test the influence of the asymmetry η (η =0.0, 0.1, 0.2) on ^{1}H-^{1}H DQ buildup curves (Fig. S2). The resulting curves of both spin systems (SS1, SS2 Fig. S2) for the different values of η are overlapping and reveal that the asymmetry has no or negligible influence on the behaviour of the DQ curves.

[1] I. Schnell, H. W. Spiess, J. Magn. Reson., 2001, **151**, 153–227.
[2] V. E. Zorin, S. P. Brown, P. Hodgkinson, Mol. Phys. 2006, **104**, 293–304.

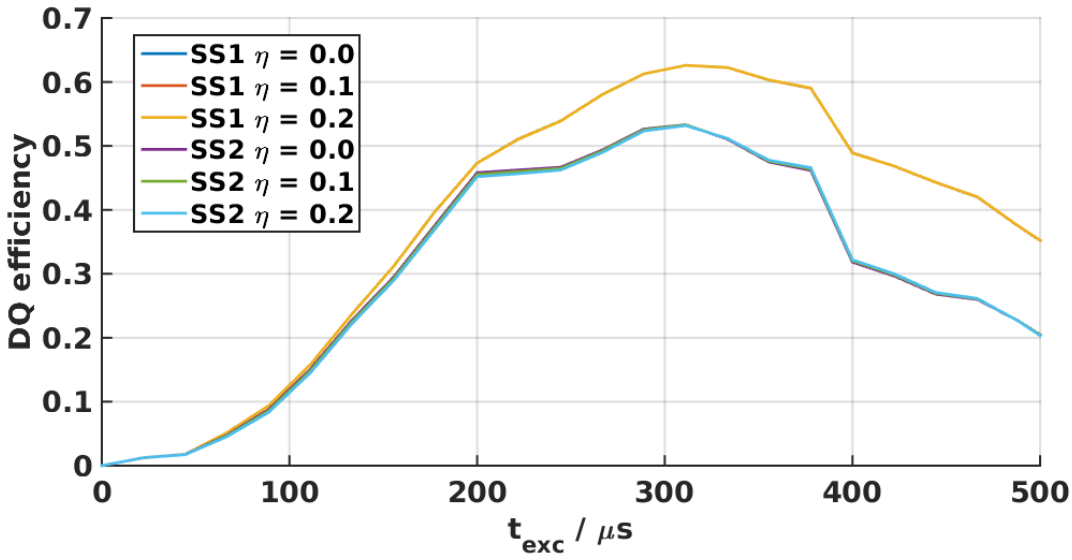

Fig. S2: Simulated ^{1}H-^{1}H DQ buildup curves ($R18_8^5$ sequence with an S_0S_π supercycle) of the spin systems SS1 and SS2 (Table S1) of an isolated Mg vacancy in ringwoodite with varying asymmetry η.

Table S1: Spin systems SS1 and SS2 of an isolated Mg vacancy in ringwoodite.

*Model V_{Mg}''+ 2H***	*^{1}H-^{1}H distance*	*δ_{iso} (H1/H2)*	*δ_{aniso} (H1/H2)*
Spin system 1 (SS1)	2.8 Å	9.1 / 8.5 ppm	-17.4 / -15.7 ppm
Spin system 2 (SS2)	2.7 Å	11.4 / 10.3 ppm	-29.2 / 21.9 ppm

2. Defect models

100 exemplary proton positions of the OH groups of each defect type extracted from the MD runs are depicted in Fig. S3. Proton H1 of the coupled defect $Mg_{Si}V_{Mg}$ "hops" after roughly 4,100 MD steps.

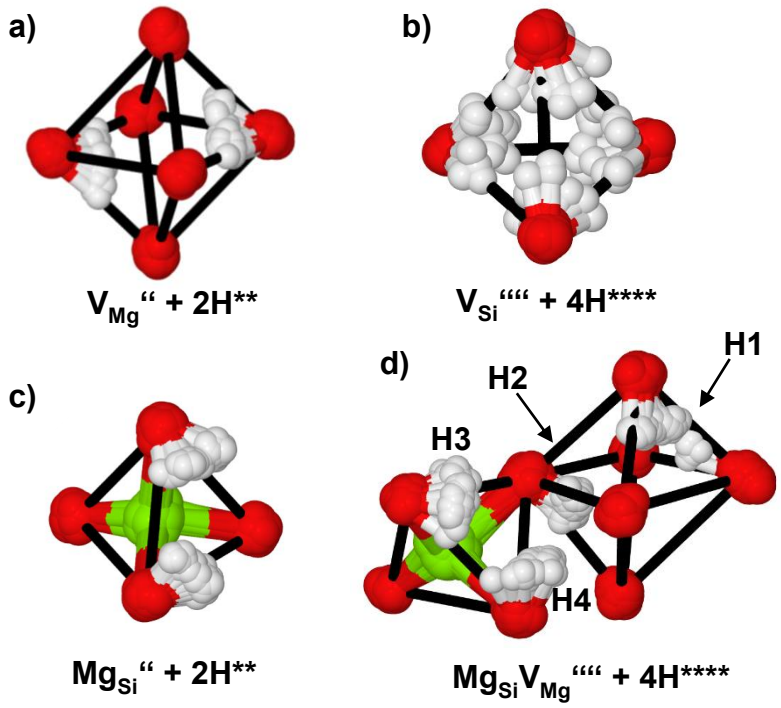

Fig. S3: 100 exemplary proton positions from the MD runs of a) an isolated Mg vacancy, b) an isolated Si vacancy charge balanced by four protons, c) an isolated Si vacancy charge balanced by an Mg^{2+} and two protons and d) a coupled defect with an octahedral vacancy and one Mg^{2+} on a Si site. In d) the four different OH groups (H1-H4) are specified. H1 has a mixed Si and Mg coordination sphere, while H2-4 are solely in Mg environment.

3. Comparison of 1D ^{1}H MAS spin echos of ringwoodite

The three 1D ^{1}H MAS spin echos of ringwoodite (Fig. S4) with interpulse delays of 25 µs (1 ν_{rot}^{-1}), 50 µs (2 ν_{rot}^{-1}, scaled by 1.15) and 75 µs (3 ν_{rot}^{-1}, scaled by 1.31) reveal that the broad components of the spectrum exhibit spin-spin relaxation times (T_2) of similar magnitude, while the sharper resonances at 1.2 and 0.8 ppm, which have previously been assigned to surface species, show slightly longer relaxations times. This behaviour allows for a quantitative description of the spectrum, since the ratio of the broad components remains virtually constant and the surface species are not considered in the description of ringwoodites defect chemistry.

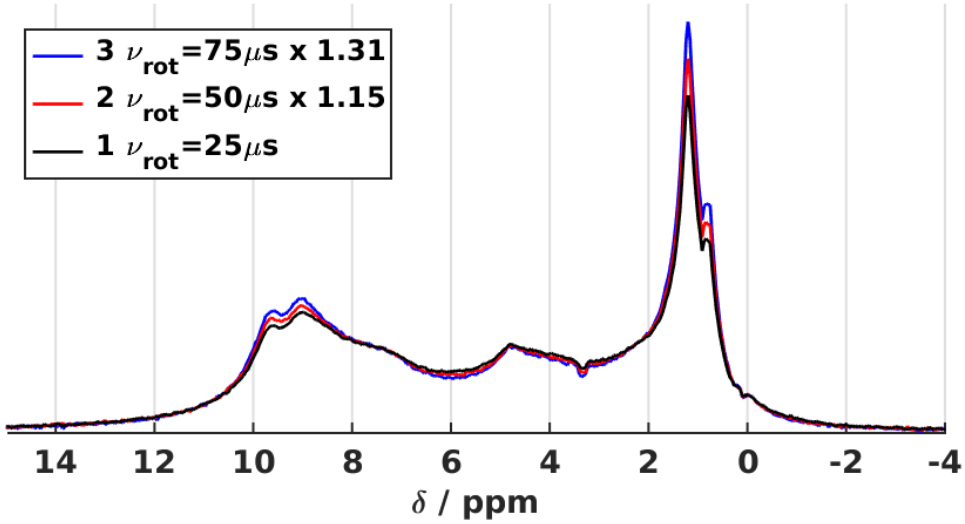

Fig. S4: Comparison of three 1D ^{1}H MAS spin echos of ringwoodite with interpulse delays of 25 µs (1 ν_{rot}^{-1}, black), 50 µs (2 ν_{rot}^{-1}, scaled up by 1.15, red) and 75 µs (3 ν_{rot}^{-1}, scaled up by 1.31, blue).

4. Simulated ^{1}H-^{1}H DQ buildup curves

The simulated individual, as well as average ^{1}H-^{1}H DQ buildup curves for the four hydrous defect types are shown in Figs. S5-S7.

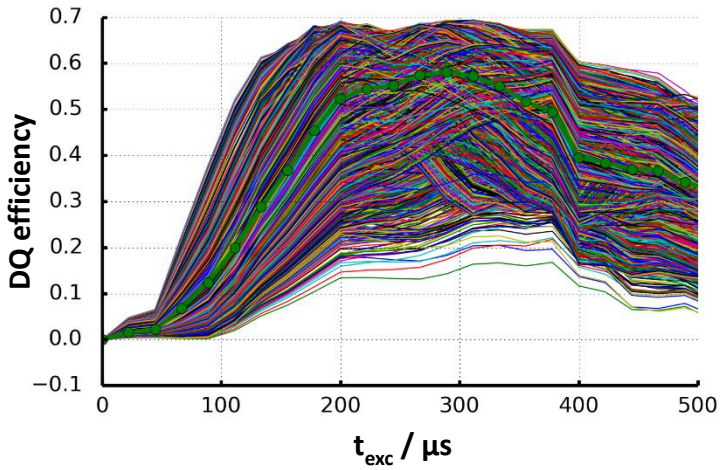

Fig. S5: Individual and averaged (green) ^{1}H-^{1}H DQ buildup curve of an isolated Mg vacancy (V_{Mg}) for the 10,000 structures of the MD run.

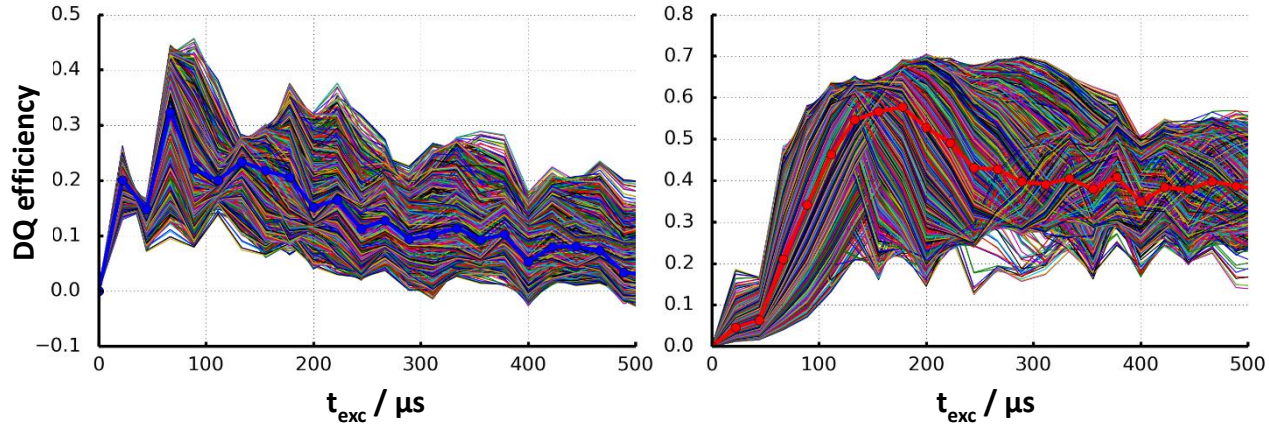

Fig. S6: Individual and averaged ^{1}H DQ buildup curve of an isolated Si vacancy charge balanced be either four protons (V_{Si}, left blue) or one Mg^{2+} and two protons (Mg_{Si}, right red) for the 10,000 structures of the MD runs.

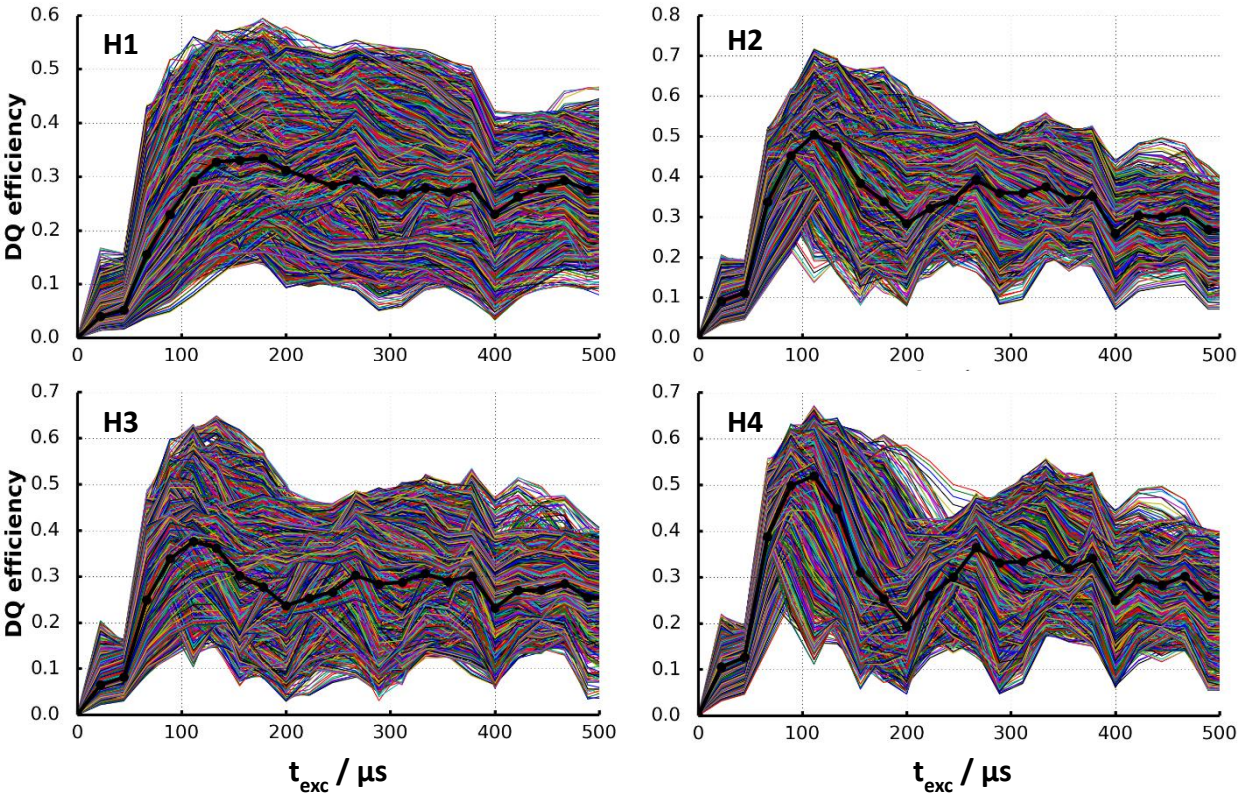

Fig. S7: Individual and averaged (black) ^{1}H-^{1}H DQ buildup curve for each OH group (H1-H4, Fig. S2) of a mixed coupled defect $Mg_{Si}V_{Mg}$ for the 10,000 structures of the MD run.

5. Convergence of ^{1}H signal and average ^{1}H-^{1}H DQ buildup curves

Figs. S8-11 show the convergence of the two experimental observables – lineshape of the ^{1}H signal and average ^{1}H-^{1}H DQ buildup curves. In each Fig. the expected ^{1}H signal or ^{1}H-^{1}H DQ build up curve is shown for increments of 1,000 MD steps. The lineshape of the ^{1}H signal (Fig. S7) for each defect type converges within 10,000 MD steps.

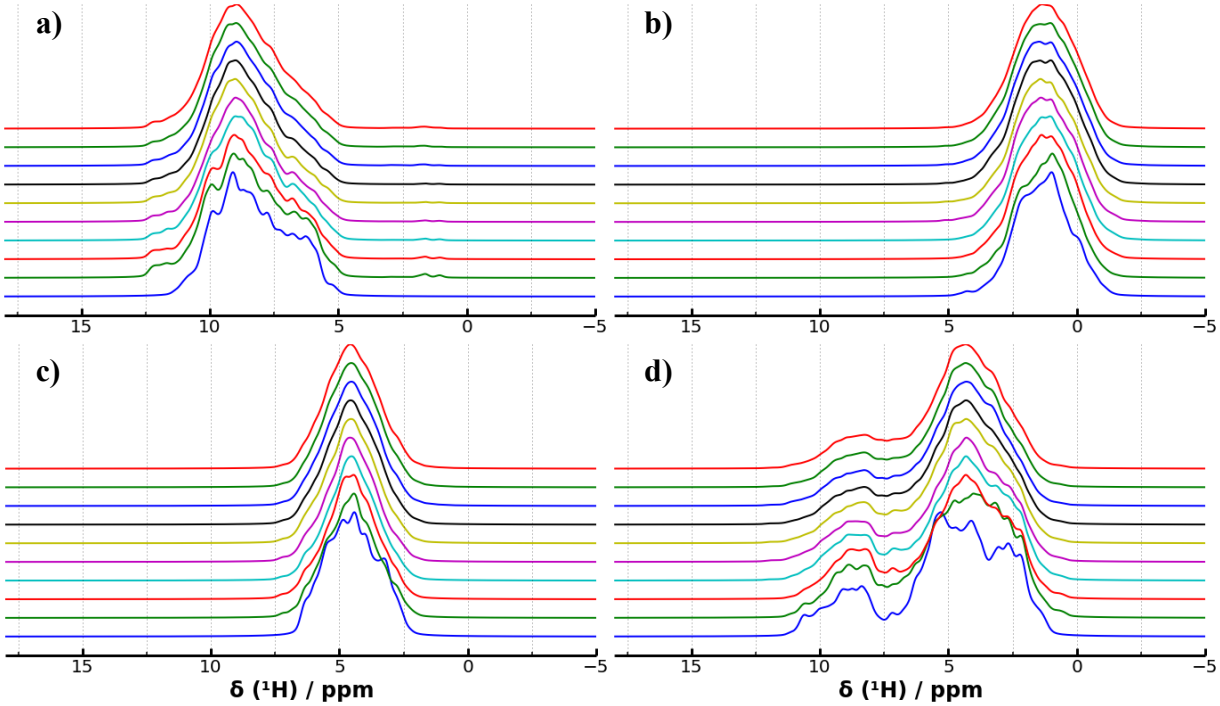

Fig. S8: Convergence of the calculated ^{1}H signal in steps of 1,000 structures for an isolated Mg vacancy (a); an isolated Si vacancy charge balanced by four protons (b) or one Mg^{2+} and two protons (c) and the mixed coupled defect (d).

The average ^{1}H-^{1}H DQ buildup curves of the isolated defect types, V_{Mg} (Fig. S9), V_{Si} and Mg_{Si} (Fig. S10) already converge after roughly 4,000 steps.

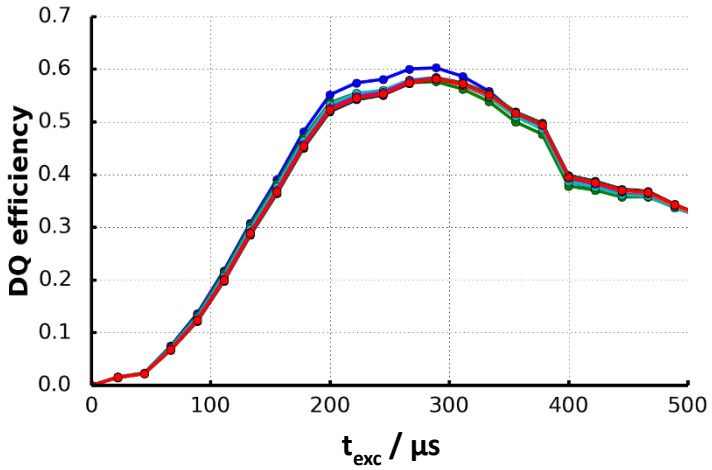

Fig. S9: Convergence of the calculated average ^{1}H-^{1}H DQ buildup curve in increments of 1,000 MD steps for an isolated Mg vacancy. The averaged curve over the first 1,000 steps is shown in blue, while the curve averaged over 10,000 structures is shown in red. Convergence of the ^{1}H-^{1}H DQ buildup curve is already reached after roughly 4,000 MD steps.

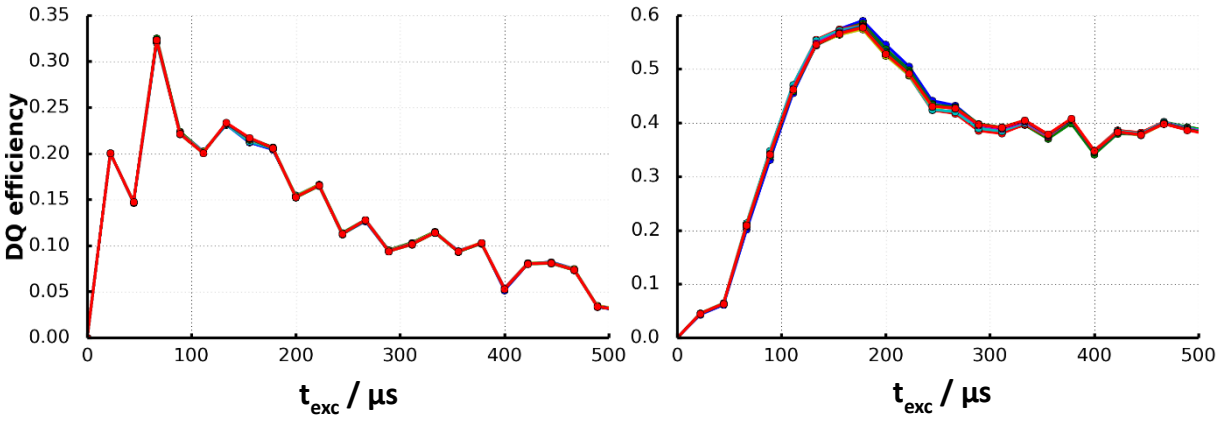

Fig. S10: Convergence of the calculated average ^{1}H-^{1}H DQ buildup curve in increments of 1,000 MD steps for an isolated Si vacancy charge balanced by four protons (left) and by one Mg^{2+} and two protons (right). The averaged curve over the first 1,000 steps is shown in blue, while the curve averaged over 10,000 structures is shown in red. Convergence of the ^{1}H ^{1}H DQ buildup curves is already reached after roughly 4,000 MD steps.

The convergence of the average ^{1}H-^{1}H DQ buildup curves of the mixed coupled defect type $Mg_{Si}V_{Mg}$ are depicted in Fig. S11. The curves take more steps (~9,000) to reach convergence since proton H1 "hops" to a neighbouring oxygen after roughly 4,100 MD steps in the simulation run.

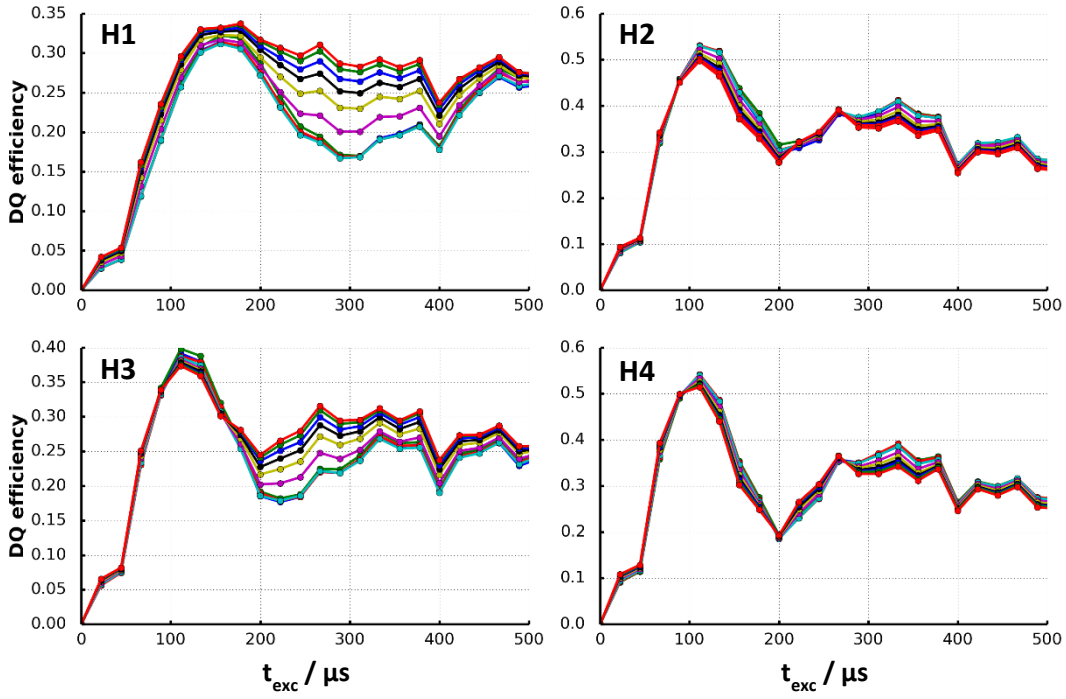

Fig. S11: Convergence of the calculated average ^{1}H-^{1}H DQ buildup curves in increments of 1,000 MD steps for the four OH groups of the mixed coupled defect $Mg_{Si}V_{Mg}$.

6. SIMPSON input for the simulation of DQ buildup curves

In the following section a representative SIMPSON input-file of one proton configuration of a V_{Mg}''+ 2H** and a one proton configuration of a $Mg_{Si}V_{Mg}''''$+ 4H**** defect model is provided. Due to the necessity to calculate points after each RR' block of the $R18_8^5$ sequence the use of propagators is not possible.

Exemplary spin-system for the V_{Mg}''+ 2H** defect model:

```
spinsys {
channels 1H
nuclei 1H 1H
shift 1 9.13519460534p -17.442954149273753p 0.0 -180.0 147.112680258 -96.0999976466
shift 2 8.45403012623p -15.721046143694831p 0.0 89.5128851082 33.9049512299 90.5869044213
dipole 1 2 -5637.1164636 0.0 31.6851345727 -78.1078876858
}
```

Exemplary spin-system for the $Mg_{Si}V_{Mg}''''$+ 4H**** defect model:

```
spinsys {
channels 1H
nuclei 1H 1H 1H 1H
shift 1 7.65570538667p -14.230231427794791p 0.0 9.56652519022e-16 89.9053170479
116.107581184
shift 2 4.83390111118p -14.91842233233166p 0.0 2.39509235681e-13 75.7896442027
145.827201686
shift 3 3.68098859231p -13.067138872028291p 0.0 180.0 72.0379085765 -115.290718781
shift 4 4.09971035372p -13.637849624820266p 0.0 -180.0 65.4909116727 -176.770801038
dipole 1 2 -9979.71504354 -0.0 90.890156288 -132.673633621
dipole 1 3 -2207.9376203 -0.0 126.834801466 -133.940698073
dipole 1 4 -1309.36099235 -0.0 121.542103199 -165.605453363
dipole 2 3 -9180.32699327 -0.0 161.606622851 -137.848273934
dipole 2 4 -3461.074725 0.0 135.429867105 161.424835593
dipole 3 4 -14279.8642363 0.0 92.4715817321 142.809597446
}
```

General Parameters and pulse program:

```
par {
variable          N 18.
variable          n 8.
variable          nu 5.
start_operator    Inz
detect_operator   I1p
spin_rate         40000
gamma_angles      5
crystal_file      zcw232
np                50
sw                spin_rate/$n
```

```
proton_frequency  600e6
verbose           11110
}


proc pulseq {} {
        global par
        maxdt 1.0

        #
        set rf [expr $par(spin_rate)*$par(N)/$par(n)]
        set p90  [expr 0.25e6/$rf]
        set p270 [expr 0.75e6/$rf]

   # Phase: phi, phi+pi, -phi, -phi+pi

        set ph10 [expr 180.00*$par(nu)/$par(N)]
        set ph11 [expr 180.00*$par(nu)/$par(N)+180.00]
        set ph12 [expr (-1)*180.00/$par(N)*$par(nu)+360.00]
        set ph13 [expr (-1)*180.00/$par(N)*$par(nu)+180.00]



# Calculation of buildup curve
# 1. Point of Buildup
reset
acq

        # 2. Point of buildup
        reset

   pulse $p90 $rf $ph10
   pulse $p270 $rf $ph11

   pulse $p90 $rf $ph12
   pulse $p270 $rf $ph13


        matrix set 1 totalcoherence {-2 2}
        filter 1

   pulse $p90 $rf $ph10
   pulse $p270 $rf $ph11

   pulse $p90 $rf $ph12
   pulse $p270 $rf $ph13


        matrix set 2 totalcoherence {0}
        filter 2
        pulseid 1 250000 -y
```

```
        acq

…. et cetera

                        }

proc main {} {
global par
set f [fsimpson]
fexpr $f {$re} {$im}
fsave $f $par(name).dat -xreim
}
```